The Astrophysical Journal, 689:1289–1294, 2008 December 20

THE EVOLVING SHAPES OF *o* CETI AND R LEONIS

K. Tatebe, E. H. Wishnow, C. S. Ryan, D. D. S. Hale, R. L. Griffith, and C. H. Townes
Space Sciences Laboratory and Department of Physics, University of California, Berkeley, CA 94720;
tatebe@ssl.berkeley.edu, wishnow@ssl.berkeley.edu, david@isi.mtwilson.edu, cht@ssl.berkeley.edu
Received 2008 April 8; accepted 2008 August 15

ABSTRACT

The sizes and shapes of the stars *o* Ceti and R Leonis have been measured in the mid-infrared. The observations were made using the UC Berkeley Infrared Spatial Interferometer (ISI), and they reveal details about the size, shape and asymmetry of both stars over several epochs in 2006. The star *o* Ceti appears to be rather symmetric, while the shape of R Leonis appears more consistent with a uniform disk plus a point source that provides approximately 9% additional intensity somewhere in the southern half of the star.

Subject headings: infrared: stars — stars: late-type — techniques: interferometric

1. INTRODUCTION

The two Mira-type stars *o* Ceti and R Leonis are both large, relatively nearby stars, making their size and shape some of the most easily measured. There is a long history of measurements at the UC Berkeley Infrared Spatial Interferometer (ISI) on both of these sources. The ISI is located on Mt. Wilson and it operates over a ~5.4 GHz bandwidth centered at 11.15 μm using heterodyne detection (Hale et al. 2000). Early ISI measurements of the sizes of these stars were made using single baseline interferometry (Danchi et al. 1994). Current long-baseline measurements use a three-telescope, triangular configuration capable of both measuring the sizes of the star along different directions and measuring asymmetries using closure phase (Hale et al. 2003). Results of closure phase measurements on the disk of α Ori have been reported previously (Tatebe et al. 2007). The results presented here for *o* Ceti and R Leo were taken during similar epochs in 2006 as the previously reported α Ori data.

2. *o* CETI

The star *o* Ceti, or Mira, is the late-type red giant for which Mira-variables are named, and it has a luminosity period of 332 days (Bowen 1990). Its change in brightness is impressive, varying from a visible magnitude around 2 down to 9, with the maximum and minimum luminosities varying somewhat from cycle to cycle. One reason that it was the first variable star seen is the relative closeness of the star, at a distance of 128^{+21}_{-15} pc (Perryman et al. 1997).

There is a large body of high spatial resolution data on Mira that spans many bands. Observations of the dust have been made at mid-infrared wavelengths by the ISI using short baselines (Bester et al. 1991; Danchi et al. 1994; Lopez et al. 1997), as well as longer, single-baseline measurements of the star by Weiner et al. (2000, 2003a) to track changes in its diameter over time. Observations have also been made by the Infrared Optical Telescope Array (IOTA; Ragland et al. 2006), the Mid-Infrared Array Camera (MIRAC3) at the NASA-IRTF (Marengo et al. 2001), and the Infrared Michelson Array (IRMA; Ridgway et al. 1992). Measurements using aperture mask interferometry have been performed at visible to near-IR wavelengths (Haniff et al. 1995; Ireland et al. 2004). Aperture mask techniques have been used at the Keck telescope in the near-IR (Woodruff et al. 2008), and segment tilting was used in the mid-IR, in addition to aperture masking on Gemini South (Ireland et al. 2007). In the ultraviolet an unusual armlike structure is seen protruding from the star (Karovska et al. 2005). Measurements of stellar size and shape by the ISI over narrow bandwidths in the mid-IR are important because of the potential distortion of apparent size by dust and spectral lines. Using mid-IR wavelengths the ISI penetrates dust reasonably well, and with a narrow bandwidth it avoids spectral lines.

Data in 2006 for October 19, 25, and 27, as well as for November 1, 2, 3, 8, 9, 10, 15, and 17 and for December 5, 6, 7, and 8 are reported with each month regarded as one epoch. The average dates for the observing epochs are 2006 October 24, November 8, and December 7. These correspond to the Julian dates JD 2,450,000+ 4033, 4047, and 4076. The corresponding phases for each of these dates are 0.64, 0.68, and 0.76, respectively. These phases are based on photometric measurements taken from the American Association of Variable Star Observers (AAVSO) database.

For the 2006 observations reported here, the three ISI telescopes were arranged in a triangle with separations of approximately 35 m. The stellar visibility and closure phase measurements were calibrated against measurements of the star α Tauri and the assumption that it is a uniform disk with a diameter of 20 mas.

For each epoch, a circular uniform disk (UD) model was fit to the data using the procedures discussed by Tatebe et al. (2007) and Tatebe (2007). Models that included asymmetry, by the addition of a point source, were also fit to the data. Fits using the asymmetric model generally yielded results with point sources of very low intensity placed in multiple locations, often outside the stellar disk. The inconsistent results indicate that the point sources probably do not fit actual characteristics of the source, such as material related to Mira B, only the noise. Thus, the best solution is that *o* Ceti is very nearly circular at a wavelength of 11.15 μm. This is somewhat surprising due to the large number of asymmetric features found in other wavelength bands. Parameters for these circular fits are shown in Table 1 for each of the three epochs.

The radii and fractions of stellar flux compared to the total flux from the star and dust for the 2006 data are plotted in Figure 1. The value for each epoch is plotted as a point, with errors, and the horizontal dotted line represents the fit using all of the data. The solid line indicates a least-squares fit to these points using a linear variation with time. The reduced χ^2 for the linear fit to the radii versus the single radius fit to all of the data are 1.14 and 6.02, respectively. For the measurements of stellar flux fraction, the sloped and flat lines have reduced χ^2 values of 2.73 and 5.25, respectively. The reduced χ^2 values indicate that the increase in size and increase in fractional brightness of the star are significant.

TABLE 1
Radius of *o* Ceti

Date (2006)	Radius (mas)	Stellar Fraction of Flux (%)	$\bar{\chi}^2$
Oct	23.14 ± 0.79	49 ± 2	1.14
Nov	22.54 ± 0.58	47 ± 1	1.35
Dec	23.91 ± 0.40	52 ± 2	0.60
All	22.98 ± 0.40	48 ± 1	1.24

Note.—The radius and fraction of stellar flux compared to the total flux of star and dust of *o* Ceti for three observation epochs and the reduced χ^2 ($\bar{\chi}^2$) of the fitted uniform disk models.

The increase in these quantities imply the data are from the latter portion of the star's cycle, when the star is growing after the minimum. Indeed, the increase in brightness shown in the AAVSO data just after the first epoch supports this. The mid-IR radius increases by about 4.7% compared to a change in visible magnitude from 8.9 to 8.4, a brightness increase of 58%. Over a full cycle the visible brightness varies by about 7 mag while the total variation at mid-infrared wavelengths is generally a magnitude or less. The fits of these uniform disk models to the October, November, and December data are shown in Figures 2–4. In all three epochs the closure phases were consistent with a rather symmetric shape.

The variation in radius is found to be consistent with the results of Weiner et al. (2003a), in which the diameter is modeled to vary sinusoidally with an amplitude of 6 mas around an average of 48 mas, and where the largest radius in the mid-infrared corresponds to a phase in the visible of 0.135. From this model, radii for the phases reported here can be estimated, and for these phases of 0.64, 0.68, and 0.76 the radii are 21.0, 21.1, and 21.9 mas. This is in reasonably good agreement with the fitted linear change in size over the three epochs shown in Figure 1 and Table 1, although the present values are somewhat larger. The discrepancy in overall size is likely due to variability in the star itself. The results of Weiner et al. (2003a) show the mean diameter to vary more than 5 mas between cycles. Data from the Diffuse Infrared Background Experiment (DIRBE) on the *COBE* satellite also indicate the maximum luminosity in the mid-infrared lags the visible by a phase of about 0.15.

The visibility data of the three baseline measurements are quite consistent with those of Weiner et al. (2003a). It is puzzling,

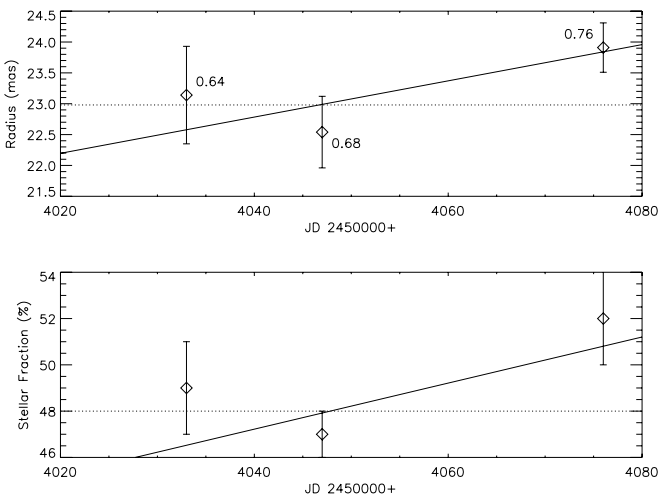

Fig. 1.—Radius and fraction of stellar flux compared to the total flux of star and dust of *o* Ceti over the three epochs in 2006 are shown in the top and bottom frames, respectively. Stellar phases at these times are given in the upper graph. Dotted lines represent means and solid lines a linear fit of the data.

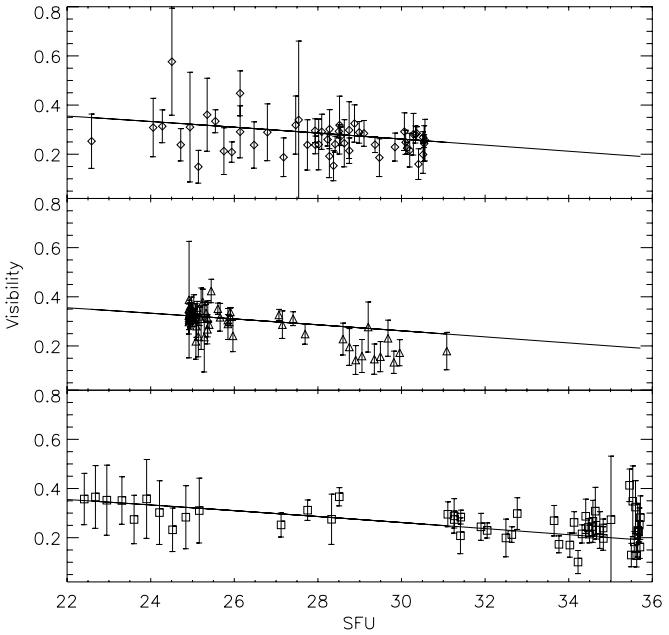

Fig. 2.—2006 October visibilities of *o* Ceti as a function of spatial frequency units, where 1 SFU = 10^5 cycles per radian. Visibility curves of the uniform disk model fit to these data are plotted as lines; the curves are the same for all three baselines. The top panel shows baseline 1-2 data (*diamonds*), the middle panel shows baseline 2-3 data (*triangles*), and the bottom panel shows baseline 3-1 data (*squares*).

however, that Mira is so nearly spherical. Although the star is often assumed to be spherical, as a simplifying assumption to theoretical analysis, most data indicate at least moderate deviations from such symmetry. Different opacity sources pertinent to various bands might be used to help reconcile this discrepancy, where some layers opaque to shorter wavelengths may be asymmetric while the layers opaque to the mid-infrared may be closer to a spherical shape. Millimeter-wave measurements by Reid & Menten (2007) also indicate a symmetric shape to within 4% and a comparable diameter of about 50 mas. Data from α Ori (Tatebe et al. 2007)

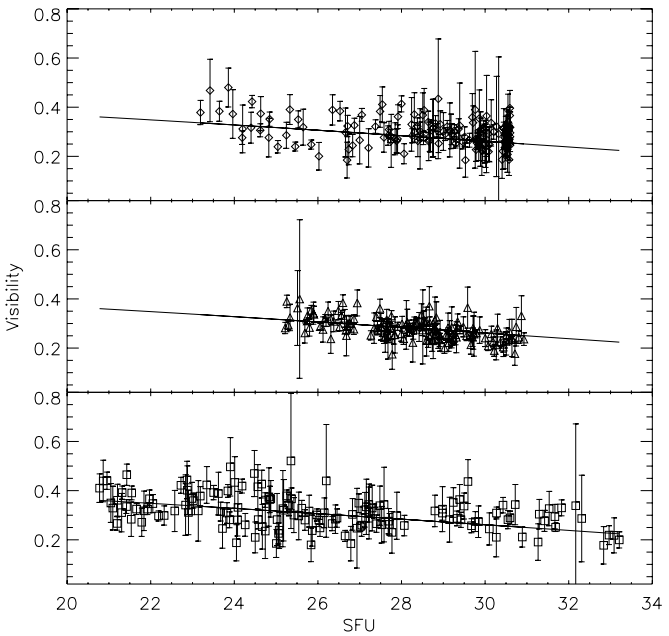

Fig. 3.—2006 November visibilities of *o* Ceti as a function of spatial frequency. The visibilities of the UD model fit to these data are plotted as lines over the data. The symbols follow the convention of Fig. 2.

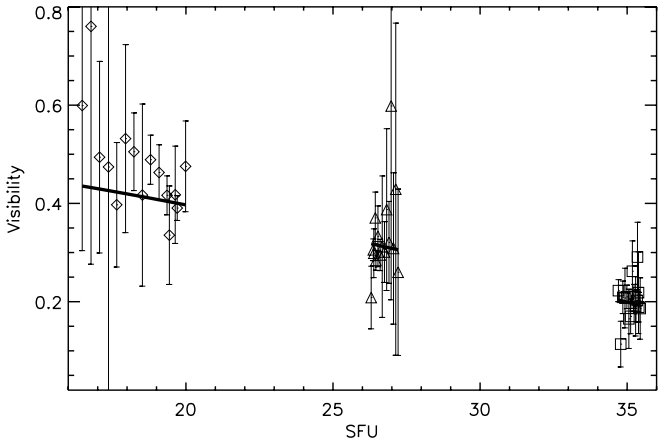

FIG. 4.—2006 December visibilities of *o* Ceti as a function of spatial frequency. The visibilities of the UD model fit to these data are plotted as lines over the data. The symbols follow the convention of Fig. 2 with the data from baselines 1-2, 2-3, and 3-1 shown from left to right, respectively.

and R Leo, however, suggest that the opacity, even in the mid-infrared, may be variable and cause the appearance of hot spots on the surface of these stars. Perhaps these spots are indeed highly variable and the surface of Mira is only temporarily quiescent.

2.1. *Possible Noncircular Shapes*

Models for *o* Ceti with some slight deviation from circular symmetry are also consistent with the data. An elliptical model can be fit to the data with comparable reduced χ^2 values. The distortion from a circle is small and only just outside the probable errors for the semimajor and semiminor radii of the ellipse. The orientation is not consistent with the elongation seen in the *HST* UV image by Karovska et al. (2005), but it aligns fairly well with the *HST* visible Faint Object Camera image of Karovska et al. (1997).

The χ^2 is not so high as to rule out a shape that is slightly distorted from a uniform disk, but to within the precision of the data reported, the star appears to be a uniform disk in 2006. Although the November data are fit reasonably well with a UD, a uniform elliptical model with a semimajor axis of 30.37 mas, a semiminor axis of 27.86 mas, and with the major axis rotated -10.84° east of north (i.e., $\sim 11^\circ$ clockwise) improves the fit slightly. The elliptical fit has a reduced χ^2 of 1.83 as compared to 1.99 for the UD model.

One striking difference between the elliptical and circular models is the fractional amount of radiation emitted by the dust. For the elliptical models the star contributes around 70% of the total flux, while the circular models have stellar fractions closer to 50%. The remainder of the radiation at 11.15 μm is due to dust.

Recently published ISI measurements made at shorter baselines indicate an asymmetric distribution of dust surrounding Mira (Chandler et al. 2007). If the surface of Mira was at times asymmetric in the past, then an uneven distribution of dust around it presently could be a result of these past asymmetries, even if the star is currently symmetric. It is also possible for turbulence to cause asymmetries in the dust shells that were symmetric when emitted.

3. R LEONIS

The M8 IIIe–type Mira variable R Leonis (R Leo) is of special importance because it is one of the most luminous Mira variables and, therefore, is one of the best studied. It has a luminosity period of 310 days. ISI observations show relatively little dust surrounding it in 2003–2004 (Tatebe et al. 2006) and a rather large diameter in the mid-infrared of 55–64 mas (Weiner et al. 2003b). Also, large changes in the relative dust-to-star intensity ratio have been seen at different phases, although the structure of the dust remains fairly unchanged between epochs. Stellar diameter measurements of R Leo are summarized in Weiner et al. (2003a) and more recent measurements in the near-IR are reported by Millan-Gabet et al. (2005).

The closure phases measured with the ISI at shorter baselines indicate that the dust surrounding the star appears rather symmetric (Tatebe et al. 2006). This might suggest that the star itself is also rather symmetric, but this does not seem to be the case. For R Leo, the dust asymmetry is not so simply correlated with stellar asymmetry. Other observations have shown asymmetry in the star's shape (Haniff et al. 1995; Perrin et al. 2004), including measurements at visible wavelengths with the *HST* (Lattanzi et al. 1997), and millimeter-wave measurements (Reid & Menten 2007).

Some past research suggests that simple symmetric models like uniform disks and basic shell models do not give a fully accurate representation of the data (Danchi et al. 1994; Schuller et al. 2004). Other measurements in the visible and near-infrared regime found R Leo to be symmetric (Hofmann et al. 2001). The visible results are uncertain, however, since the dust shell that surrounds the star can absorb radiation and produce, among other effects, uneven limb darkening. This makes 11.15 μm measurements by the ISI particularly interesting as the stellar atmosphere is observable directly with minimal obscuration by dust.

R Leonis was observed on 2006 November 8, 10, 15, 16, and 20 and on December 5, 6, 7, 14, 15, and 20. Significant changes in size are apparent between these two epochs. A nonzero closure phase is measured on the star, although with somewhat large errors; the closure phase measurements are shown in Figure 7 (*bottom*). The exact value of the closure phase also depends on the bandwidth over which the fringe is measured, where this is presumably due to noise. Although the scatter of the closure phase measurements is substantial, more than half the points lie within $\pm 45^\circ$. A weighted average of the closure phase data is $10.96^\circ \pm 2.12^\circ$ and a simple average assuming uniform errors is $8.54^\circ \pm 3.12^\circ$. A conservative estimate of the average closure phase taking into account both interpretations is $9.3^\circ \pm 3.8^\circ$. This error is stated under the assumption that the closure phase has a constant value over the range measured; however, the UD plus point source models that are fitted to the data do not have constant closure phases as a function of position angle.

To characterize the changes in the star, the data sets from November and December are modeled separately using an elliptical model. The major and minor radii and orientations of the star are given in Table 2. At a distance of 101 pc (Perryman et al. 1997), a radius of 30.0 mas is equivalent to 4.53×10^{11} m or 3.03 AU. Over the two epochs, both the semimajor and semiminor radii increased by $\sim$2.35 mas indicating an even swelling of the star in both directions. This suggests, as accepted theory states, that the star pulsates in a radially symmetric breathing mode. This also indicates that the observed ellipticity is probably not generated by this oscillation since radial modes have azimuthal symmetry. It is not clear from available data whether this radial oscillation is the fundamental radial mode or one of higher frequency, and it is difficult to determine the frequencies of the modes based on simple models, since estimating the frequencies requires an accurate estimate of the star's mass and distance. The picture is further complicated by turbulence in the stellar atmosphere.

The orientation of the ellipse's semimajor axis varies between the two measurements in 2006, but this variation is within the errors of these parameters and is not well constrained by the data. The general northerly direction of the elongation axis corresponds reasonably well with the elliptical shape shown in Figure 2 of

TABLE 2
Elliptical Models of R Leo

Date	A (mas)	B (mas)	θ (deg)	Stellar Fraction of Flux (%)	$\bar{\chi}^2$
Nov	29.03 ± 0.34	27.40 ± 0.39	-2.1 ± 23.0	55 ± 4	1.58
Dec	32.31 ± 0.21	30.63 ± 0.25	19.0 ± 12.0	80 ± 4	1.53
All	31.81 ± 0.15	30.67 ± 0.22	-4.3 ± 14.2	75 ± 4	1.71

Notes.— Parameters of uniform ellipses fit to R Leo for the two periods of observation and the combined data. The major and minor radii are denoted as A and B, respectively. Here θ is the orientation angle of the semimajor axis rotated towards the east from north (counterclockwise).

Reid & Menten (2007). The radii in the east-west direction agree well with results from Weiner et al. (2003a,) which reported radii of 27.7 ± 2.5 and 31.12 ± 0.5 mas at phases of 0.43 and 0.77, respectively. The radii measurements given in Table 2 were taken at phases of 0.66 and 0.74 in November and December, respectively, where phases were determined using AAVSO data. The visible brightness of R Leo at a phase of 0.43 is not very different from the brightness at a phase of 0.66. This suggests the radius of R Leo might be roughly the same at these two phases, and indeed, the current measurement of 27.4 mas at a phase of 0.66 compares favorably to the measurement by Weiner et al. (2003a) of 27.7 mas at a phase of 0.43. The 30.6 mas radius measured at a stellar phase of 0.74 also corresponds well to the 31.1 mas radius measured by Weiner et al. (2003a) at a stellar phase of 0.77. Recent 2007 ISI measurements, obtained at approximately the same phase as in 2006, show a radius essentially the same as that reported here for 2006.

The parameters of an ellipse fitted to the combined data set are also included in Table 2, where the fit to an ellipse is not as good as for the individual data sets. The fit to the combined data set is dominated by the December data due to a significantly larger number of observations. The elongations of the elliptical model fits of R Leo for November and December are approximately 6%, whereas that of the combined data set is ~4%. This is less than the 17% elongation found for the star α Ori (Tatebe et al. 2007). Even so, it is greater than might be expected from the distortion of a giant star caused by rotation, if a rotational speed similar to that of α Ori is assumed. Furthermore, the measured 9.3° closure phase indicates that hot spots are a better explanation than elongation, as an elliptical shape has center-of-inversion symmetry, and hence a closure phase of zero.

3.1. *Point-Source Asymmetry*

Combining the data from the two epochs in 2006 provides nonzero closure phase with greater significance, but the averaging obscures temporal variations of the visibility data. To take advantage of the closure phase information, asymmetric models are fitted to the full 2006 data set. The asymmetry and orientation of these models are then compared to the pure ellipses as a consistency check.

Two models, a uniform disk with one point source and a uniform disk with two point sources, are fit to the combined data set. These models are shown in Figures 5 and 6, and the parameters of these models are listed in Table 3. Figure 7 shows the visibility data and the closure phase data. The visibility curves from the two models are plotted over the data as solid and dashed curves for the single- and double-point models, respectively. Since the models are asymmetric, each baseline has a different fitted visibility curve. Each panel of the visibility plot shows six curves, many of which overlap to the point of being indistiguishable. In each panel, the upper curve indicates the modeled visibilities for baseline 1-2 (*red*); the lower curve consists of a coincidental overlap between the 2-3 (*blue*) and 3-1 (*green*) visibilities. The corresponding dashed curves overlap the solid curves almost exactly, but the dashed curve can be seen to the left in the top frame and to the right in the bottom frame. In the lower closure phase plot (*magenta*), the single-point (*solid curve*) and double-point models (*dashed curve*) are more easily distinguished. The radii of the two asymmetric models in Table 3 are in rough accord with those found in the elliptical models above, and the added points are generally in line with the elongation of the elliptical models. Two models are used to help gain a greater intuitive understanding of the nature of the asymmetry. Using more than two points did not significantly improve the fit and any additional points were of small intensity.

The two asymmetric models show that there is an excess of intensity to the south side of the star. The morphology of the intensity excess is uncertain, since the single-point source in the first model and the widely separated pair of points in the second both fit the data about equally well. The large errors associated with the two-point model indicate how poorly constrained the actual location and size of the asymmetry is, although the total amount of flux contained in the points is about the same between the two models: ~9.5%. These comparisons indicate the error for the location of the single point in the first model is somewhat underestimated. The small error is likely an artifact of the point's small size causing sharp changes in the χ^2 with position. These errors represent how rapidly χ^2 increases as the point is moved a small amount from its stated location. In reality, the behavior of χ^2 as the point-source location varies is complex. While χ^2 increases rapidly in the immediate vicinity of the point, there are many

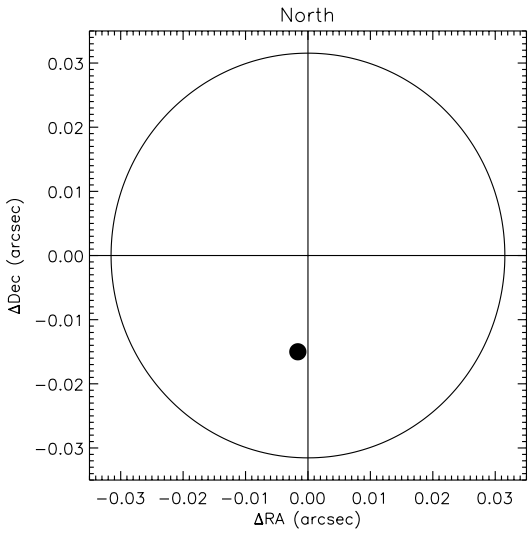

Fig. 5.— Uniform disk with a single point source model of R Leo fit to the full set of 2006 measurements. North is up, and east is left.

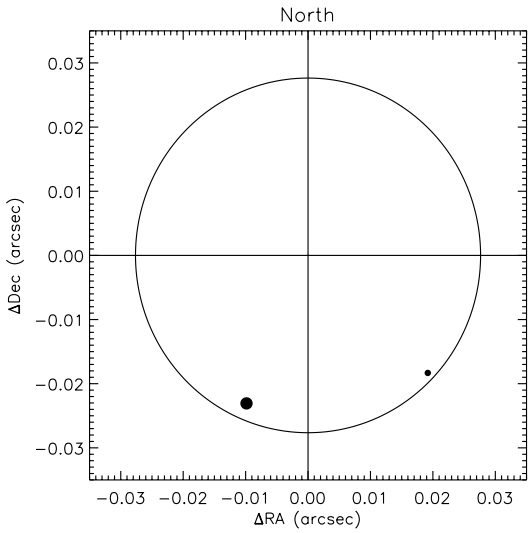

FIG. 6.— Uniform disk and two point sources model of R Leo fit to the full set of 2006 measurements. North is up, and east is left.

nearby locations that give χ^2 values that are almost as small as the best fit. The errors in the intensities of the individual points for the two-point model are rather large and it is difficult to directly estimate the error in the sum of these quantities from the errors of the quantities separately. Both models, however, have similar amounts of total intensity contained in the point sources, as mentioned above. The consistency of the total flux between models indicates the error in the total of the two-point model is probably near the error in the flux for the single-point model: ~2.5%.

The flux represented by the point sources is also of comparable magnitude to the point source in the model of α Ori (Tatebe et al. 2007). This suggests that the same mechanisms may be at work to generate the asymmetry, and favors a hot spot interpretation for both stars, rather than a protuberance. This is because a protuberance, if it is the same temperature as the rest of the stellar surface, can only be seen if it peeks beyond the edge of the stellar disk. If a protuberance extends from the stellar surface only toward the observer, then no features will be seen since there will be no observable change in brightness across the stellar disk. By contrast, a hot spot is brighter than the surface of the star, and it will be apparent when seen against the stellar disk regardless of its location.

4. RELATIVE SIZE OF *o* CETI AND R LEONIS AT MILLIMETER AND 11.15 μm WAVELENGTHS

The sizes of *o* Ceti and R Leo at 43 GHz (0.697 cm) have recently been published (Reid & Menten 2007), with major and minor axes for *o* Ceti given as 54 ± 5 and 50 ± 5 mas, and those for R Leo 61 ± 10 and 39 ± 6 mas, respectively. These are notably similar to the sizes reported here at a wavelength of 11.15 μm. This is curious, since the apparent size is expected to be significantly larger in the microwave compared to the mid-infrared.

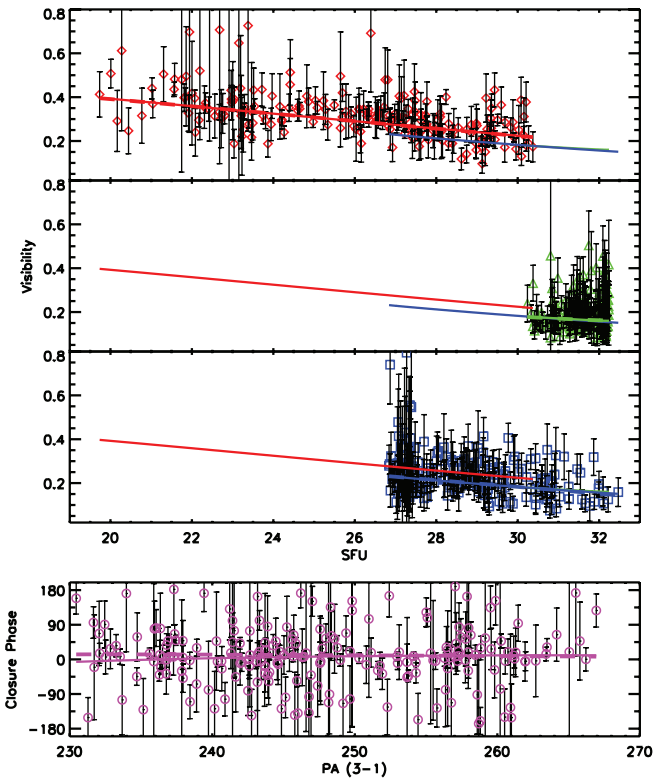

FIG. 7.— Visibilities and closure phases of R Leo from the full 2006 measurement set. In the top panel, the upper plot shows baseline 1-2 (*red*) data, the middle plot shows baseline 2-3 (*green*) data, and the lower panel shows baseline 3-1 (*blue*) data. The bottom panel shows the closure phases (*magenta*) as a function of the baseline 3-1 position angle. Visibilities for the models in Figs. 5 and 6 are shown as solid and dashed lines, respectively, and they are plotted in each panel where colors refer to the respective baselines. The two model visibility curves almost completely overlap, but the distinction between closure phase curves is apparent.

Opacity at both of these wavelengths is believed to be dominated by electron-hydrogen collisions, with the absorption coefficient per centimeter given by (Reid & Menten 1997; Tatebe et al. 2006)

$$\alpha = \frac{kTn_e n_{\rm H} A}{\nu^2}, \qquad (1)$$

TABLE 3
MODEL PARAMETERS FOR R LEO IN 2006

Parameter	Circle and One Point	Circle and Two Points
$\bar{\chi}^2$	1.58	1.57
Stellar fraction of flux (%)	49.7 ± 2.7	47.2 ± 25.7
Stellar radius (mas)	31.5 ± 1.7	27.6 ± 3.6
Percent flux from point 1	9.3 ± 2.5	6.6 ± 21.1
Point 1 location *x* (mas)	−1.6 ± 1.0	−9.9 ± 15.6
Point 1 location *y* (mas)	−15.0 ± 1.2	−23.1 ± 19.4
Percent flux from point 2	...	3.4 ± 7.2
Point 2 location *x* (mas)	...	19.2 ± 14.3
Point 2 location *y* (mas)	...	−18.3 ± 6.4

NOTE.— Parameters for the models shown in Figs. 5 and 6.

where n_e and n_H are densities of electrons and hydrogen atoms respectively, ν is the frequency, and A is 10^3 at a temperature of 2300 K, varying only $\pm 25\%$ for temperatures between 1500 and 3000 K. Since n_e is closely proportional to n_H, the absorption coefficient or opacity is proportional to $(Tn_H^2 A)/\nu^2$. From this, for a given opacity per unit distance at a fixed temperature, n_H must be proportional to ν, and for the same opacity, the density at the effective stellar radius for $\lambda = 0.697$ cm must be smaller than that at the stellar radius for $\lambda = 11.15 \times 10^{-4}$ cm by the inverse ratio of the wavelengths, or almost a factor of 625.

If the stellar atmosphere is in thermal equilibrium, the density should be proportional to $e^{(mMG)/(RkT)}$, where m is the hydrogen atomic mass, M and R are the stellar mass and radius, respectively, and G the gravitational constant. Assuming M equals a solar mass, and the distance to o Ceti is 110 pc, then the stellar diameter of 48 mas implies a radius of 3.95×10^{13} cm and at a temperature of 1700 K this factor is $e^{24.0}$. The apparent stellar size would require the opacity multiplied by the stellar radius to have close to the same value at both wavelengths. Hence, for a change in density of a factor of 625 as required by the 0.697 cm versus 11.15 μm wavelengths, R should change by a factor 1.37. This is an approximation, assuming that the temperature does not vary with radius. One might alternately assume that the total flux is constant, which implies that $T \propto R^{-1/2}$. In that case R should change still more, by a factor of 1.87. The measured change in stellar size with wavelength is much smaller, the ratio of diameter measurements by Reid & Menten (2007) at 0.697 cm to these results at 11.15 μm being $\approx 52/46.3 = 1.123$.

Of course, the size of o Ceti changes with time, and present measurements at 11.15 μm were made in approximately 2006 November, at a phase near 0.70, while those of Reid and Menten were made in approximately 2000 November, at a phase of 0.05. Fortunately, there were earlier measurements at 11.15 μm by the ISI system (Weiner et al. 2003a) which showed a diameter of approximately 47.5 mas in 2000 November, the same time as when the Reid and Menten measurements were made. This would give a ratio of 1.095, even a little smaller than the above one.

The remarkably similar diameters of o Ceti at the two very different wavelengths, with a ratio of about 1.1 rather than 1.3 or more expected from an atmospheric in thermal equilibrium, shows that the gas surrounding o Ceti may not be in thermal equilibrium. Alternatively, there may be aspects of the opacity mechanisms at the two wavelengths that are still not fully understood. Presumably, gas is blown off by dynamic effects of the star or its atmosphere, making the decrease in density with distance from the star much more rapid than that expected from thermal equilibrium. Data for R Leo at the two wavelengths are not quite as complete as that for o Ceti. However, the measurement at 0.69 cm of maximum and minimum diameters 61 ± 10 and 39 ± 6 mas, respectively (Reid & Menten 2007), and present measurements at 11.15 μm of approximately 58 mas, show a similar phenomenon, that also for this star the stellar atmosphere decreases in density much more rapidly than is expected from thermal equilibrium.

5. CONCLUSIONS

The sizes and shapes two Mira-type stars, o Ceti and R Leo, have been measured using interferometric techniques. Size measurements of o Ceti agree well with previous ISI results and the star varies in size with stellar phase as expected. These measurements, however, indicate that o Ceti is remarkably symmetric, a fact that is striking considering the pronounced asymmetries found in o Ceti in other wavelength bands, as well as the asymmetries of other Mira-type stars in the mid-infrared. Furthermore, it is somewhat puzzling how the asymmetric dust shells found around o Ceti are generated from such a symmetric source. The other Mira-type star presented here, R Leo, shows significant asymmetry and, along with previous results for α Ori, indicates that asymmetries in late-type stars may be common. The measured asymmetry of R Leo is consistent with a uniform disk with an extra amount of intensity somewhere in the southern hemisphere of the star. Further measurements to track the changes in the sizes and shapes of these stars over a longer period will be helpful in better understanding the mechanisms that generate these asymmetries. The sizes of both stars measured at approximately 0.7 cm and 11.15×10^{-4} cm differ by rather small amounts, indicating atmospheres that decrease in density much more rapidly than would be expected from thermal equilibrium.

We acknowledge use of *Hipparcos* data obtained from the Simbad database, visible photometry from the AAVSO, and infrared photometry from the LAMBDA-DIRBE database. We are very grateful for support from the Office of Naval Research, the National Science Foundation, and the Gordon and Betty Moore Foundation.

REFERENCES

Bester, M., Danchi, W. C., Degiacomi, C. G., Townes, C. H., & Geballe, T. R. 1991, ApJ, 367, L27
Bowen, G. H. 1990, in Proc. NATO Advanced Research Workshop on the Numerical Modelling of Nonlinear Stellar Pulsations, ed. J. R. Buchler (Dordrecht: Kluwer), 155
Chandler, A. A., Tatebe, K., Wishnow, E. H., Hale, D. D. S., & Townes, C. H. 2007, ApJ, 670, 1347
Danchi, W. C., et al. 1994, AJ, 107, 1469
Hale, D. D. S., et al. 2000, ApJ, 537, 998
———. 2003, Proc. SPIE, 4838, 387
Haniff, C. A., Scholz, M., & Tuthill, P. G. 1995, MNRAS, 276, 640
Hofmann, K.-H., Balega, Y., Scholz, M., & Weigelt, G. 2001, A&A, 376, 518
Ireland, M. J., Tuthill, P. F., Bedding, T. R., Robertson, J. G., & Jacob, A. P. 2004, MNRAS, 350, 365
Ireland, M. J., et al. 2007, ApJ, 662, 651
Karovska, M., Hack, W., Raymond, J., & Guinan, E. 1997, ApJ, 482, L175
Karovska, M., Schlegel, E., Hack, W., Raymond, J. C., & Wood, B. E. 2005, ApJ, 623, L137
Lattanzi, M. G., Munari, U., Whitelock, P. A., & Feast, M. W. 1997, ApJ, 485, 328
Lopez, B., et al. 1997, ApJ, 488, 807
Marengo, M., Karovska, M., Fazio, G. G., Hora, J. L., Hoffmann, W. H., Dayal, A., & Deutsch, L. K. 2001, ApJ, 556, L47
Millan-Gabet, R., Pedretti, E., Monnier, J. D., Schloerb, F. P., Traub, W. A., Carleton, N. P., Lacasse, M. G., & Segransan, D. 2005, ApJ, 620, 961
Perrin, G., et al. 2004, A&A, 426, 279
Perryman, M. A. C., et al. 1997, A&A, 323, L49
Ragland, S., et al. 2006, ApJ, 652, 650
Reid, M. J., & Menten, K. M. 1997, ApJ, 476, 327
———. 2007, ApJ, 671, 2068
Ridgway, S. T., Benson, J. A., Dyck, H. M., Townsley, L. K., & Hermann, R. A. 1992, AJ, 104, 2224
Schuller, P., et al. 2004, A&A, 418, 151
Tatebe, K. 2007, Ph.D. thesis, Univ. California, Berkeley
Tatebe, K., Chandler, A. A., Hale, D. D. S., & Townes, C. H. 2006, ApJ, 652, 666
Tatebe, K., Chandler, A. A., Wishnow, E. H. Hale, D. D. S., & Townes, C. H. 2007, ApJ, 670, L21
Weiner, J., Danchi, W. C., Hale, D. D. S., McMahon, J., Townes, C. H., Monnier, J. D., & Tuthill, P .G. 2000, ApJ, 544, 1097
Weiner, J., Hale, D. D. S., & Townes, C. H. 2003a, ApJ, 588, 1064
———. 2003b, ApJ, 589, 976
Woodruff, H. C., Tuthill, P. G., Monnier, J. D., Ireland, M. J., Bedding, T. R., Lacour, S., Danchi, W. C., & Scholtz, M. 2008, ApJ, 673, 418